minerals

MDPI

Article

Chemical Composition of Mn- and Cl-Rich Apatites from the Szklary Pegmatite, Central Sudetes, SW Poland: Taxonomic and Genetic Implications

Adam Szuszkiewicz [1,*], Adam Pieczka [2], Bożena Gołębiowska [2], Magdalena Dumańska-Słowik [2], Mariola Marszałek [2] and Eligiusz Szełęg [3]

[1] Institute of Geological Sciences, University of Wrocław, pl. M. Borna 9, 50-204 Wrocław, Poland
[2] Department of Mineralogy, Petrography and Geochemistry, AGH University of Science and Technology Mickiewicza 30, 30-059 Kraków, Poland; pieczka@agh.edu.pl (A.P.); goleb@agh.edu.pl (B.G.); dumanska@uci.agh.edu.pl (M.D.-S.); mmarszal@agh.edu.pl (M.M.)
[3] Department of Geochemistry, Mineralogy and Petrography, Faculty of Earth Sciences, University of Silesia, Będzińska 60, 41-200 Sosnowiec, Poland; eligiusz.szeleg@us.edu.pl
* Correspondence: adam.szuszkiewicz@uwr.edu.pl

Received: 6 July 2018; Accepted: 9 August 2018; Published: 14 August 2018

Abstract: Although calcium phosphates of the apatite group (*apatites)* with elevated contents of Mn are common accessory minerals in geochemically evolved granitic pegmatites, their Mn-dominant analogues are poorly studied. Pieczkaite, $^{M1}Mn_2{}^{M2}Mn_3(PO_4)_3{}^{X}Cl$, is an exceptionally rare Mn analogue of chlorapatite known so far from only two occurrences in the world, i.e., granitic pegmatites at Cross Lake, Manitoba, Canada and Szklary, Sudetes, SW Poland. In this study, we present the data on the compositional variation and microtextural relationships of various *apatites* highly enriched in Mn and Cl from Szklary, with the main focus on compositions approaching or attaining the stoichiometry of pieczkaite (*pieczkaite-like apatites*). The main goal of this study is to analyze their taxonomical position as well as discuss a possible mode of origin. The results show that *pieczkaite*-like *apatites* represent the Mn-rich sector of the solid solution $^{M1}(Mn,Ca)_2{}^{M2}(Mn,Ca)_3(PO_4)_3{}^{X}(Cl,OH)$. In the case of cation-disordered structure, all these compositions represent extremely Mn-rich hydroxylapatite or pieczkaite. However, for cation-ordered structure, there are also intermediate compositions for which the existence of two hypothetical end-member species can be postulated: $^{M1}Ca_2{}^{M2}Mn_3(PO_4)_3{}^{X}Cl$ and $^{M1}Mn_2{}^{M2}Ca_3(PO_4)_3{}^{X}OH$. In contrast to hydroxylapatite and pieczkaite, that are members of the apatite-group, the two hypothetical species would classify into the hedyphane group within the apatite supergroup. The *pieczkaite*-like *apatites* are followed by highly Mn-enriched fluor- and hydroxylapatites in the crystallization sequence. Mn-poor chlorapatites, on the other hand, document local contamination by the serpentinite wall rocks. We propose that *pieczkaite*-like *apatites* in the Szklary pegmatite formed from small-volume droplets of P-rich melt that unmixed from the LCT-type (Li–Cs–Ta) pegmatite-forming melt with high degree of Mn-Fe fractionation. The LCT melt became locally enriched in Cl through in situ contamination by wall rock serpentinites.

Keywords: pieczkaite; Mn-rich apatite; apatite supergroup; granitic pegmatite; Szklary; Sudetes

1. Introduction

The apatite supergroup includes minerals with the generic formula $^{IX}M1_2{}^{VII–IX}M2_3(TO_4)_3X$. The two distinct *M* sites may incorporate a wide range of cations—Ca^{2+}, Pb^{2+}, Ba^{2+}, Sr^{2+}, Mn^{2+}, Na^{+}, Ln^{3+} (lanthanides), Y^{3+}, Bi^{3+}; while $T = P^{5+}$, As^{5+}, V^{5+}, Si^{4+}, S^{6+}, B^{3+}; and $X = F^{-}$, OH^{-}, Cl^{-}, and O^{2-}. Very diverse chemical compositions within the supergroup result in a number of mineral species formally divided into five crystal-chemical groups [1]: apatite group (both *M* sites

dominated by the same cation; *T* = P, V or As), hedyphane group (*M* sites dominated by different cations; *T* = P, As or S), belovite group (*M*1 site split into distinct *M*1 and *M*1′ sites dominated by different cations; *M*2 = Sr; *T* = P), britholite group (cations only partially ordered between the two *M* sites, typically contain lanthanides; *T* = Si), and ellestadite group (*T* = Si and S with 1:1 ratio). The most common among the apatite-supergroup minerals are the calcium phosphates, with the general formula $Ca_2Ca_3(PO_4)_3(F,Cl,OH)$, a group that includes three distinct species of fluor-, chlor-, and hydroxylapatites with anion solid solutions between them [2,3]. In this contribution, the term *apatites* will be henceforth used to denote such phosphates with unlimited degrees of Mn↔Ca and F↔Cl↔OH substitutions. Species names will be applied when referring to specific compositions. *Apatites* are very common accessory minerals in granitic pegmatites and enrichment in Mn is typically observed, particularly in geochemically more evolved pegmatitic bodies [2]. Nonetheless, pegmatitic *apatites* with Mn > 1 *apfu* are quite rare and they typically are fluorapatites [4–6].

Pieczkaite, ideally $^{M1}Mn_2{}^{M2}Mn_3(PO_4)_3{}^{X}Cl$, is an exceptionally rare mineral of the apatite group, defined as the Mn analogue of chlorapatite $Ca_5(PO_4)_3Cl$, pyromorphite $Pb_5(PO_4)_3Cl$ and alforsite $Ba_5(PO_4)_3Cl$. Pieczkaite was first described on the basis of a crystal with the empirical formula: $(Mn_{3.36}Fe_{0.20}Ca_{1.40})_{\Sigma 4.96}(P_{1.01}O_4)_3(Cl_{0.62}OH_{0.38})_{\Sigma 1.00}$ from a pegmatitic occurrence at Cross Lake, Manitoba, Canada [7]. To our knowledge, the only other confirmed occurrence of apatite-group minerals with Mn > Ca and Cl-dominated *X* site is a granitic pegmatite at Szklary, Lower Silesia, Poland, from which a mineral with the composition $(Mn_{2.43}Ca_{2.29}Fe^{2+}{}_{0.24}Mg_{0.04}Na_{0.01})_{\Sigma 5.01}(PO_4)_3(Cl_{0.48}F_{0.32}OH_{0.20})_{\Sigma 1.00}$, close to pieczkaite, has been described [8]. However, in contrast to the Cross Lake pieczkaite, the pieczkaite-like mineral from Szklary was tentatively allocated to the hedyphane group with a supposed end-member formula $Mn_2Ca_3(PO_4)_3Cl$, on the assumption that Mn and Ca are ordered at the *M*1 and *M*2 sites, respectively [1]. In this contribution, we present new data on the chemical composition of *apatites* from the Szklary pegmatite with compositions approaching or attaining the composition of pieczkaite. Their crystallochemical relationships, taxonomical position, and a possible mode of formation are discussed and potentially new members of the apatite supergroup are proposed.

2. Geological Setting and Mineralogical Description of the Szklary Pegmatite

The Central Sudetes constitute a mosaic of continent- and ocean-related tectono-stratigraphic units, located in Lower Silesia (SW Poland) at the northeastern edge of the Bohemian Massif in the eastern part of the European Variscan Belt (Figure 1). These tectono-stratigraphic units have recently been interpreted as fragments of a Variscan accretionary complex, squeezed during the Variscan collision between the two peri-Gondwanan microcontinents of Saxo-Thuringia in the west and Brunia in the east, intruded by late to post-Variscan granitoids and partly covered by Late Paleozoic sequences of intramontane basins (see [9,10] for details and further references). The central position in this region is occupied by the high-grade metamorphic complex of the Góry Sowie Block (GSB), interpreted as a fragment of the Saxo-Thuringian lower continental crust [11]. The GSB contains abundant granitic pegmatites of rare-element class that crystallized from melts produced by partial melting of a metasedimentary-metavolcanic rock suite during amphibolite facies metamorphism ~380–370 Ma [12–15]. The GSB unit is bordered on the north-east, east, and south by an assemblage of weakly metamorphosed mafic-ultramafic complexes of the ~400 Ma Central-Sudetic Ophiolite [16–19]. Some authors have suggested also that ophiolitic rocks at least partly underlie GSB (e.g., [20–23]). It is generally regarded that the obducted ocean-related lithologies and the crustal-related GSB rock suites were already in contact in the Late Devonian [24]. The Szklary Massif, ~10 km long and up to 3 km wide, represents a part of the dismembered Central-Sudetic Ophiolite that adjoins GSB on the east and is enclosed as a mega-boudin in the mylonitized Góry Sowie gneisses of the Early Carboniferous Niemcza Shear Zone (Figure 1). The Szklary Massif is mainly composed of serpentinized peridotites, with minor amphibolites, lamprophyres, rodingites, plagiogranites, and anorthosites [25–28]. Dioritic dikes, identified in drill cores in the north-eastern part of the massif, are traditionally related (e.g., [25])

to small volume late-syntectonic dioritic, syenitic, and granodioritic intrusions that penetrated the Niemcza Shear Zone at ~335–340 Ma [17,29]. The rock suite of the Szklary massif is cut by veins of secondary silica-carbonate mineralization and extensive tertiary weathering led to the formation of a nickeliferous weathering cover.

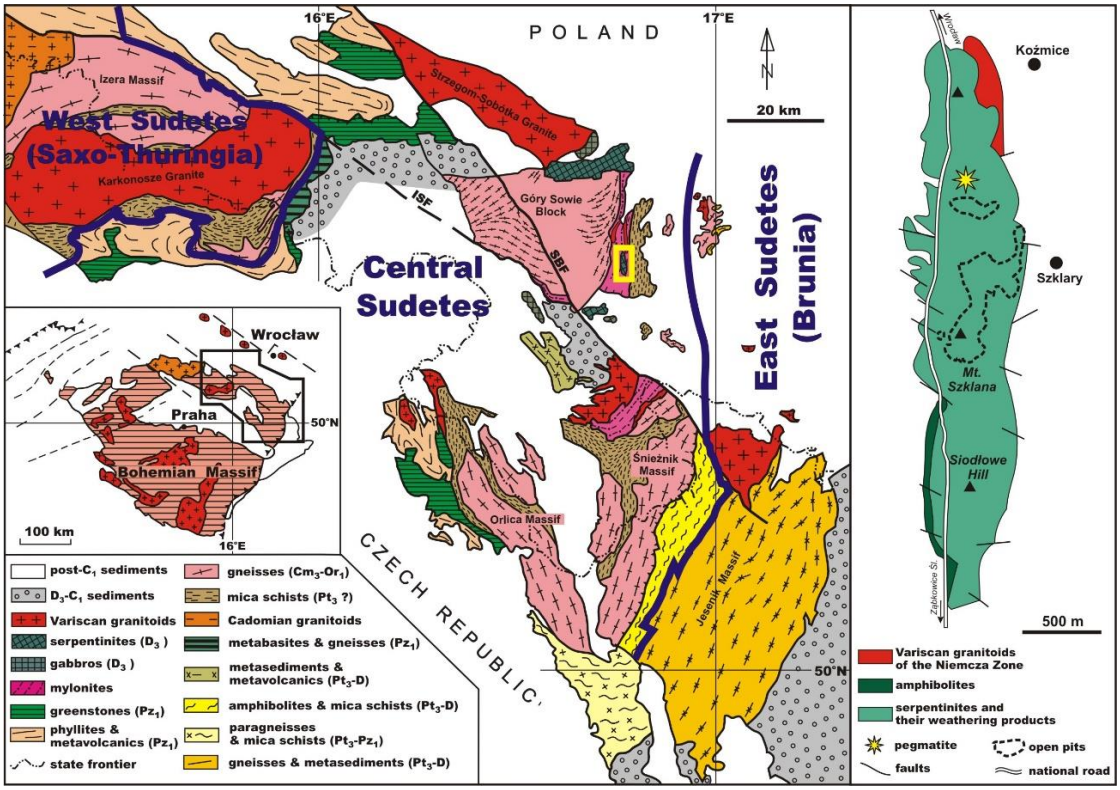

Figure 1. Geological sketch map of the Sudetes and its position in the Bohemian Massif (after [10], simplified). Yellow rectangle marks the position of the Szklary Massif. The right inlet shows the geology of the Szklary Massif with the location of the Szklary pegmatite (after [30], modified). Abbreviations: ISF—Intra Sudetic Fault, SBF—Sudetic Boundary Fault.

The Szklary granitic pegmatite has an affinity for the beryl–columbite–phosphate subtype of the *REL*–Li class and LCT (***Li***–***Cs***–***Ta***) geochemical family *sensu* [31]. The enrichment in P and the LCT affinity of the pegmatite point to metasedimentary source rocks for the pegmatite-forming melt (e.g., [32]). It is considered that the Szklary pegmatite is a product of an anatectic melt generated in the adjacent GSB unit [33,34]. Age determinations support this view, showing that the pegmatite formed at ~383 ± 3 Ma (CHIME dating on monazite) [34], contemporaneously with the pegmatite-producing anatectic event in GSB. The Szklary pegmatite crops out on the NE scarp of the abandoned "Marta" nickel mine (50°39′ N; 16°50′ E), in the northern part of the Szklary Massif, ~6 km north of the Ząbkowice Śląskie town, Lower Silesia, SW Poland (Figure 1) and is now nearly completely mined out by mineral collectors. The pegmatite forms a NNE–SSW elongated lens or a boudin, ~4 × 1 × 3 m large. It is in primary intrusive contact with an up to 2 m thick body of aplitic gneiss to the southwest and both rocks are surrounded by tectonized serpentinite. Locally, a thin tabular body of amphibolite, ~10–30 cm thick, occurs close to the eastern pegmatite-serpentinite contact. Sometimes, the pegmatite contains centimetre-sized partly or nearly completely digested amphibolite and serpentinite xenoliths. A vermiculite-chlorite-talc zone is locally present along the contact with serpentinite. The pegmatite consists mostly of sodic plagioclase (An ≤ 14%), microcline, quartz, and *biotite*, with minor Fe^{3+}-bearing schorl-dravite tourmaline and muscovite. It is poorly zoned with, ideally: (1) a few centimetres thick marginal quartz-feldspar graphic unit with *biotite* and black tourmaline; (2) a coarser-grained

intermediate graphic unit (microcline > plagioclase; individual feldspar crystals rarely exceed 15 cm across) enriched in muscovite and tourmaline (schorl–foitite) and containing accessory chrysoberyl; and (3) a *biotite*-free central graphic zone containing locally developed blocky feldspar segregations (microcline >> plagioclase; individual crystals in blocky feldspar segregations up to ~5 cm across) and occasional aggregates of tourmaline [33,34]. A quartz core is absent. Transitions between the units are gradational and the proportion between zones 2 and 3 varies. K-feldspar and plagioclase are slightly enriched in P (~0.57 wt % P_2O_5 on average) and the K-feldspar contains up to 0.20 wt % Rb_2O [33]. *Biotite* is generally altered to Fe-rich clinochlore with minor vermiculite and talc. Muscovite shows no significant enrichment in Li and F [33]. A number of accessory minerals form grains, usually below 1 mm in size, disseminated in the internal zone of the pegmatite [34–38]. They include: native elements and alloys (As, Sb, Bi, Au, stibarsen, and paradocrasite), Nb–Ta oxides (columbite-group minerals, stibiocolumbite and stibiotantalite, fersmite, pyrochlore-, microlite-, and betafite-group minerals), Mn-oxides (ernienickelite, jianshuiite, cesàrolite, cryptomelane, and others), As and Sb oxides, beryllium minerals (chrysoberyl, beryl, and bertrandite), monazite-(Ce), Dy-bearing xenotime-(Y), (Be,Mn)-bearing cordierite, tourmaline-group minerals (dravite/schorl grading to foitite/oxy-schorl), dumortierite-supergroup minerals, spessartine garnet, zircon, pollucite, and others. The Szklary pegmatite is a type locality for nioboholtite, titanoholtite, and szklaryite [37]. A characteristic feature of the pegmatite is the presence of an assemblage rich in Mn- and Pb-bearing phosphates, such as: Mn-rich fluor-, hydroxyl-, and chlorapatites, beusite, beusite-(Ca), pieczkaite, bobfergusonite, fillowite, lithiophilite grading to sicklerite, simferite and purpurite, natrophilite, Ba- and Pb-bearing dickinsonites, triploidite, fairfieldite, phosphohedyphane, plumbogummite, mitridatite, and probably robertsite [34,38,39]. Only *apatites* and beusites are up to 1–2 cm in size while others form inclusions ranging from 200–100 μm in size in *apatites*, beusites, microcline, muscovite, and quartz.

3. Sample Description and Paragenetic Position

In the Szklary pegmatite, fluor- and hydroxylapatites with the Mn content only occasionally slightly exceeding 1 *apfu* are relatively common accessory phosphates in all the pegmatitic units. They have been described [8,33] and will be referred to as *common apatites*. This paper is focused on much less frequent *apatites* highly enriched in Mn and Cl and the research material includes also other atypical *apatites* associated with them. On textural and compositional grounds, the *apatites* can be divided into several types.

Type 1 includes *apatites* with compositions approaching or attaining the stoichiometry of pieczkaite, free of fluorine, or containing this component in subordinate amounts. This type is found almost exclusively in the intermediate zones of the pegmatite, as irregular grains, up to ~200 μm in size, usually in complex intergrowths with beusites (Figure 2A) and sometimes accompanied also by bobfergusonite and fillowite (samples Sz26, Sz31, and Sz108). These intergrowths are of primary origin and are typically strongly altered to a mixture of secondary Mn-oxides and smectites [8]. Single euhedral crystals of Type 1 *apatites* (sample Sz79), ~100 μm long, are found only exceptionally within coarsely crystalline muscovite (Figure 2B).

Texturally distinct Type 2 is represented by some patchy-zoned anhedral crystals (sample Sz29) that consist of a mosaic of domains enriched in Mn and Cl and patches with markedly lower concentrations of Mn but still enriched in Cl (Figure 2C). Some compositions of Type 2 *apatites* also show the presence of increasing F. We interpret this complex zoning pattern as not resulting from processes of metasomatic alteration but as a primary feature indicative of disequilibrium crystallization.

In many cases, the Type 1 *apatites* (samples Sz53, Sz94, and Sz97), alone or together with beusites, are overgrown or partly replaced by Type 3 *apatites* (Figure 2D). Type 3 is characterized by much lower, though still elevated, contents of Mn coupled to a significant content of F and often an absence of Cl. Textural observations suggest that in the crystallization sequence: (1) Type 1 *apatites* with or without beusites were followed first by (2) patchy-zoned crystals of Type 2 and finally by (3) Type 3.

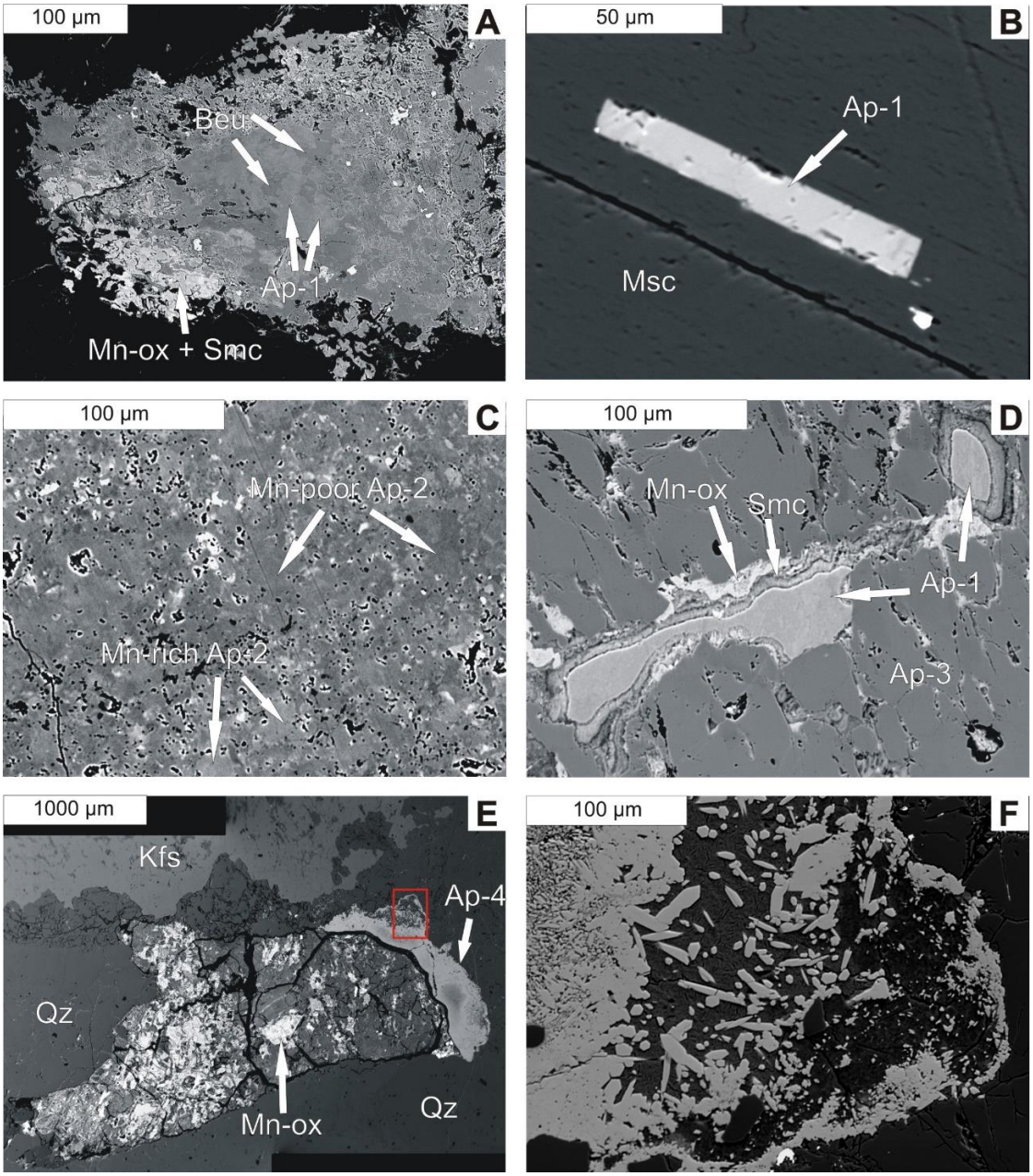

Figure 2. BSE (backscattered electron) images of *apatites* from the Szklary pegmatite. (**A**) Type 1 *apatite* with stoichiometry of pieczkaite intergrown with beusite and partly altered to secondary smectites and Mn oxides (sample Sz108); (**B**) Euhedral Type 1 *apatite* in muscovite (sample Sz79); (**C**) Patchily zoned Type 2 *apatite* with the domains compositionally similar to Type 1 intergrown with Cl-rich domains of markedly lower Mn contents and trace amounts of F (sample Sz29); (**D**) A relic of the Type 1 *apatite* rimmed by secondary smectites and Mn oxides and overgrown by Type 3 of Mn-rich fluor- to hydroxylapatite; (**E**) Panorama for a strongly digested relic of a serpentinite xenolith with Type 4 *apatite* (sample Sz132) formed along its margin. Red box marks the area enlarged and rotated in the image F; (**F**) Aggregate of the Type 4 crystal with the composition of Mn-poor chlorapatite. Abbreviations: Ap 1–4: *apatites* of Types 1–4 (further explanation in the text), Beu: beusite, Mn-ox: Mn oxides, Smc: smectite, Msc: muscovite, Qz: quartz, Kfs: potassic feldspar.

In order to discuss possible sources of Cl-enrichment in the crystals, we also analyzed another atypical *apatite* (sample Sz132) that shows very high content of Cl but a negligible amount of Mn (Figure 2E,F). This Type 4 *apatite* was found as clusters of up to ~50 µm large euhedral crystals along

the margin of a nearly completely digested serpentinite xenolith in the outer zone of the pegmatite. However, the Type 4 *apatites* are not a part of the mineral assemblage with Types 1–3 *apatites* and their textural position suggests that the compositions are largely controlled by elements supplied from the dissolving xenolith.

4. Methods

Fragments of the pegmatite were mounted in resin on 1 inch discs and coated with carbon. Electron-microprobe analyses (EPMA) were performed at the Inter-Institute Analytical Complex for Minerals and Synthetic Substances of the University of Warsaw with a CAMECA SX Five FE field emission electron probe microanalyser operating in the wave-dispersive mode under the following conditions: acceleration voltage 20 kV, beam current 15 nA, beam diameter 2 μm, peak count-time 20 s, background count-time 10 s. Standards, analytical lines, diffracting crystals, and mean detection limits (in wt %) were as follows: fluorophlogopite (FK_α, LPC0, 0.10), albite (NaK_α, LPC0, 0.04), diopside (MgK_α, TAP, 0.02), (SiK_α, TAP, 0.03) and (CaK_α, LPET, 0.02), apatite (PK_α, LPET, 0.03), tugtupite (ClK_α, LPET, 0.02), orthoclase (KK_α, LPET, 0.02), rhodonite (MnK_α, LLIF, 0.05), hematite (FeK_α, LLIF, 0.05), $SrBaNb_4O_{12}$ (SrK_α, TAP, 0.05), and GaAs (AsL_α, TAP, 0.06). The raw data were ZAF-reduced. The empirical formulae are normalized in relation to 12 O + (F + Cl + OH) atoms per formula unit (*apfu*). Such elements as V and Cr were not detected by EPMA and As was detected only in Mn-poor chlorapatite (sample Sz132). The effect of possible replacement of PO_4^{3-} by MnO_4^{3-} or BO_3^{3-}, although not verifiable by EPMA, is regarded as insignificant. Traces of Na, K, and Sr are accepted in the formula calculations only if the analyzed amounts diminished by 2 standard deviations for ~95% confidential level exceed the respective detection limits. In order to suppress the effect of potential migration of F and Cl along the sixfold *c* axis [40], extended exposure time to an electron beam was avoided. Where possible, we analyzed grains oriented perpendicular to *c* axis (e.g., sample Sz79; Figure 2B) because the effect of halogens migration is minimal in this orientation [41]. However, in the case of small anhedral grains, this was usually not possible and the analyses were obtained in random orientations. The content of OH^- is calculated assuming full occupancy of the *X* site and neglecting the presence of ions or molecules other than F^- and Cl^- (e.g., O^{2-}, H_2O and others). Although these simplifications may lead to some errors in the estimations of the *X*-site occupants, it does not influence the main line of our reasoning. The analyses of beusite that co-occurs with the *apatites* were normalized to 8O *apfu*.

5. Chemical Composition

Concentration ranges of selected elements in Types 1–4 *apatites* from the Szklary pegmatite are shown in Figure 3 and Table 1. Representative chemical compositions of Type 1 are given in Table 2 and of Types 2–4 in Table 3. In Type 1 *apatites,* two main components, MnO and CaO, vary widely from 28.52 to 51.73 wt % and from 4.71 to 27.79 wt %, respectively (2.19–4.24 Mn *apfu* and 0.48–2.70 Ca *apfu*). The concentration of FeO varies from 0.61 to 7.00 wt % ($\leq$0.56 Fe *apfu*), while MgO, SrO, Na_2O and K_2O occur in trace amounts and do not exceed, respectively, 0.47 wt % (0.06 *apfu*), 1.41 wt % (0.07 *apfu*), 0.33 wt % (0.06 *apfu)* and 0.17 wt % (0.02 *apfu*). Fluorine, up to 0.36 wt % (0.10 *apfu*) and 0.46 wt % (0.13 *apfu*), was detected in only two samples with the lowest Mn contents (Sz31 and Sz79). The contents of 2.45–5.14 wt % Cl (0.38 to 0.83 Cl *apfu*) indicate that the remaining *X* site position is filled with 0.17–0.59 OH *apfu*.

Table 1. Concentration ranges of selected elements from various textural-paragenetic types of *apatites* from the Szklary pegmatite. Sz26 = sample, #Mn = Mn/(Mn + Fe), b.d.l. = below detection limit. For definition of Types 1–4 see the text.

	Type 1	**Type 1**	**Type 1**	**Type 1**	**Type 1**	**Type 1**	**Type 1**	**Type 2**	**Type 3**	**Type 3**	**Type 3**	**Type 4**
wt %	Sz26	Sz31	Sz53	Sz79	Sz94	Sz97	Sz108	Sz29	Sz53	Sz94	Sz97	Sz132
P_2O_5	35.44–39.11	38.98–39.44	36.34–36.98	37.38–39.07	36.97–39.42	35.58–37.73	35.49–38.66	38.87–40.41	40.47–41. 02	39.93–40.34	40.71–40.80	38.54–39.71
As_2O_5	b.d.l.	b.d.l.	b.d.l.	b.d.l.	b.d.l.	b.d.l.	b.d.l.	b.d.l.	b.d.l.	b.d.l.	b.d.l.	0.99–2.06
FeO	1.71–3.67	2.72–3.15	1.61–3.18	1.43–2.24	0.61–4.61	1.87–5.21	1.90–7.00	0.19–1.25	0.37–0.60	0.27–0.59	0.30–0.38	0.40–0.82
MnO	33.51–51.73	30.04–31.78	43.17–48.18	28.52–33.57	30.59–47.03	38.73–48.49	37.50–47.39	10.61–23.68	18.62–19.87	17.36–19.25	18.26–19.17	1.46–1.99
MgO	0.03–0.37	0.12–0.27	0.00–0.08	0.07–0.15	0.05–0.27	0.04–0.19	0.02–0.47	b.d.l.	0.03–0.07	b.d.l.	b.d.l.	b.d.l.
CaO	4.71–22.80	23.66–24.64	8.41–13.10	20.97–27.79	7.79–26.10	5.45–17.49	5.82–18.70	31.80–45.04	37.64–39.89	37.44–39.40	37.77–38.43	51.67–53.91
SrO	0.00–0.64	b.d.l.	0.00–0.34	b.d.l.	0.00–1.41	0.00–0.55	0.00–0.93	0.00–1.61	b.d.l.	b.d.l.	b.d.l.	0.09–0.34
Na_2O	0.00–0.13	0.00–0.07	0.00–0.21	b.d.l.	0.00–0.24	0.13–0.29	0.00–0.33	0.00–0.04	0.00–0.04	b.d.l.	b.d.l.	0.20–0.38
K_2O	0.00–0.12	b.d.l.	b.d.l.	0.10–0.17	b.d.l.	b.d.l.	b.d.l.	b.d.l.	b.d.l.	b.d.l.	b.d.l.	b.d.l.
F_2	b.d.l.	0.29–0.46	b.d.l.	0.13–0.36	b.d.l.	b.d.l.	b.d.l.	0.00–1.21	1.61–2.12	1.45–2.21	1.25–2.35	b.d.l.
Cl_2	4.07–5.14	3.00–3.29	3.90–4.32	2.45–2.97	3.02–4.89	3.86–4.76	2.62–4.92	1.98–4.58	0.00–0.03	b.d.l.	0.11–0.20	3.07–5.08
apfu												
P^{5+}	2.95–3.06	2.99–3.01	2.98–3.00	2.98–3.02	2.97–3.01	2.95–3.03	2.97–3.04	2.98–3.00	2.98–3.00	2.98–3.00	3.00–3.01	2.85–2.93
As^{5+}												0.05–0.09
F^-		0.08–0.13		0.04–0.10				0.00–0.34	0.44–0.58	0.41–0.62	0.34–0.65	
Cl^-	0.64–0.83	0.46–0.51	0.64–0.71	0.38–0.47	0.46–0.79	0.62–0.78	0.41–0.79	0.29–0.71	0.00		0.02–0.03	0.45–0.75
$OH^-_{(cal.)}$	0.17–0.36	0.37–0.43	0.29–0.36	0.45–0.53	0.21–0.54	0.22–0.38	0.21–0.59	0.29–0.58	0.42–0.56	0.38–0.59	0.34–0.63	0.25–0.55
Fe^{2+}	0.13–0.28	0.21–0.24	0.13–0.26	0.11–0.18	0.05–0.33	0.15–0.42	0.15–0.56	0.01–0.09	0.03–0.04	0.02–0.04	0.02–0.03	0.03–0.06
Mn^{2+}	2.62–4.24	2.32–2.44	3.53–3.91	2.19–2.69	2.33–3.81	3.06–3.94	2.95–3.80	0.79–1.80	1.35– 1.46	1.29–1.44	1.35–1.42	0.11–0.15
Mg^{2+}	0.00–0.05	0.02–0.04	0.00–0.01	0.01–0.02	0.01–0.04	0.01–0.03	0.00–0.06		0.00–0.01			
Ca^{2+}	0.48–2.26	2.29–2.40	0.86–1.34	2.12–2.70	0.80–2.52	0.56–1.75	0.59–1.85	3.10–4.22	3.49–3.67	3.57–3.71	3.53–3.60	4.85–4.97
Sr^{2+}	0.00–0.03		0.00–0.02		0.00–0.07	0.00–0.03	0.00–0.05	0.00–0.08				0.00–0.02
Na^+	0.00–0.02	0.00–0.01	0.00–0.04		0.00–0.04	0.02–0.05	0.00–0.06	0.00–0.01	0.00–0.01			0.03–0.05
K^+	0.00–0.01			0.01–0.02								
#Mn	0.92–0.96	0.91–0.92	0.94–0.96	0.94–0.95	0.90–0.98	0.90–0.96	0.84–0.95	0.95–0.98	0.97–0.98	0.97–0.99	0.98–0.99	0.70–0.79

Table 2. Representative chemical compositions and proposed cation distributions (dominant components are bold) between the *M*1 and *M*2 sites in the Type 1 *apatites* from the Szklary pegmatite. Sz26/35 = sample/analysis, b.d.l. = below detection limit, Ca* = Ca + Sr + Na + K, Mn* = Mn + Fe + Mg, #Mn = Mn/(Mn + Fe) and #Mn* = Mn*/(Mn* + Ca*). Further explanations in the text.

wt %	Sz26/11	Sz26/35	Sz31/10	Sz31/4	Sz53/2	Sz53/15	Sz79/1B	Sz79/3B	Sz79/6B	Sz79/11B	Sz94/55	Sz94/57	Sz97/27B	Sz97/34B	Sz108/106	Sz108/19
$P_2O_{5(cal.)}$	36.75	38.23	38.98	39.12	36.96	36.94	38.07	38.57	38.87	38.81	38.04	37.11	37.83	37.21	36.73	38.32
FeO	2.39	1.71	3.14	2.98	2.69	1.71	2.18	1.74	1.58	1.69	1.01	4.18	2.00	3.48	5.97	1.90
MnO	51.73	33.51	30.04	31.12	48.18	43.60	33.19	30.56	28.52	30.46	34.35	47.03	38.73	48.49	46.57	37.96
MgO	0.08	0.03	0.27	0.15	0.03	b.d.l.	0.13	0.11	0.10	0.10	0.07	0.16	0.05	0.08	0.19	0.02
CaO	5.01	22.80	24.56	24.11	8.41	13.10	22.58	25.56	27.79	25.32	21.22	7.79	17.49	6.80	6.74	18.70
SrO	b.d.l.	0.37	b.d.l.	b.d.l.	b.d.l.	b.d.l.	b.d.l.	b.d.l.	b.d.l.	b.d.l.	0.64	0.28	0.55	b.d.l.	b.d.l.	0.35
Na_2O	b.d.l.	b.d.l.	b.d.l.	0.07	0.10	b.d.l.	b.d.l.	b.d.l.	b.d.l.	b.d.l.	0.22	0.17	0.16	0.29	b.d.l.	b.d.l.
K_2O	b.d.l.	b.d.l.	b.d.l.	b.d.l.	b.d.l.	b.d.l.	0.14	0.12	0.14	0.12	b.d.l.	b.d.l.	b.d.l.	b.d.l.	b.d.l.	b.d.l.
F_2	b.d.l.	b.d.l.	0.34	0.29	b.d.l.	b.d.l.	0.19	0.28	0.36	0.36	b.d.l.	b.d.l.	b.d.l.	b.d.l.	b.d.l.	b.d.l.
Cl_2	4.70	4.85	3.29	3.16	4.27	4.06	2.90	2.57	2.45	2.59	4.01	4.87	3.91	4.27	4.62	4.74
$H_2O_{(cal.)}$	0.35	0.39	0.65	0.71	0.48	0.53	0.79	0.85	0.86	0.81	0.59	0.33	0.61	0.47	0.38	0.42
$-O=F_2$	0.00	0.00	−0.14	−0.12	0.00	0.00	−0.08	−0.12	−0.15	−0.15	0.00	0.00	0.00	0.00	0.00	0.00
$-O=Cl_2$	−1.06	−1.09	−0.74	−0.71	−0.96	−0.92	−0.65	−0.58	−0.55	−0.58	−0.91	−1.10	−0.88	−0.96	−1.04	−1.07
Total	99.95	100.80	100.39	100.87	100.16	99.03	99.44	99.66	99.97	99.53	99.24	100.81	100.44	100.14	100.17	101.34
apfu																
$PO_4^{3-}{}_{(cal.)}$	3.01	2.99	3.00	3.00	3.00	2.99	2.98	2.99	2.99	3.00	3.01	3.00	2.99	3.02	3.00	3.00
F^-			0.10	0.08			0.05	0.08	0.10	0.10						
Cl^-	0.77	0.76	0.51	0.49	0.69	0.66	0.46	0.40	0.38	0.40	0.64	0.79	0.62	0.69	0.75	0.74
$OH^-{}_{(cal.)}$	0.23	0.24	0.39	0.43	0.31	0.34	0.49	0.52	0.52	0.50	0.36	0.21	0.38	0.31	0.25	0.26
Ca^{2+}	0.52	2.26	2.40	2.34	0.86	1.34	2.24	2.51	2.70	2.48	2.12	0.80	1.75	0.70	0.70	1.85
Sr^{2+}		0.02									0.03	0.02	0.03			0.02
Mn^{2+}	4.24	2.62	2.32	2.39	3.91	3.54	2.60	2.37	2.19	2.36	2.72	3.81	3.06	3.94	3.80	3.97
Fe^{2+}	0.19	0.13	0.24	0.23	0.22	0.14	0.17	0.13	0.12	0.13	0.08	0.33	0.16	0.28	0.48	0.15
Mg^{2+}	0.01	0.00	0.04	0.02	0.00		0.02	0.01	0.01	0.01	0.01	0.02	0.01	0.01	0.03	0.00
Na^+				0.01	0.02						0.04	0.03	0.03	0.05		
K^+							0.02	0.01	0.02	0.01						
#Mn	0.96	0.95	0.91	0.91	0.95	0.96	0.94	0.95	0.95	0.95	0.97	0.92	0.95	0.93	0.89	0.95
#Mn*	0.90	0.55	0.52	0.53	0.82	0.73	0.55	0.50	0.46	0.50	0.56	0.83	0.64	0.85	0.86	0.63
^{M1}Ca*	0.00	**1.55**	**1.22**	**1.07**	0.00	0.32	0.78	0.95	**1.16**	**1.01**	**1.10**	0.21	0.67	0.00	0.00	**1.10**
^{M1}Mn*	**1.97**	0.48	0.77	0.93	**2.01**	**1.70**	**1.26**	**1.08**	0.88	0.99	0.90	**1.80**	**1.37**	**1.98**	**2.01**	0.89
^{M2}Ca*	0.52	0.72	1.18	1.29	0.88	1.02	1.47	**1.57**	**1.56**	1.49	1.09	0.64	1.14	0.75	0.70	0.77
^{M2}Mn*	**2.48**	**2.28**	**1.82**	**1.71**	**2.12**	**1.98**	**1.53**	1.43	0.44	**1.51**	**1.91**	**2.36**	**1.86**	**2.25**	**2.30**	**2.23**

Table 3. Representative chemical compositions of Types 2–4 apatites and proposed cation distributions (dominant components are bold) between the M1 and M2 sites in Type 2 apatites from the Szklary pegmatite. Sz29/16 = sample/analysis, b.d.l. = below detection limit, Ca* = Ca + Sr + Na + K, Mn* = Mn + Fe + Mg, #Mn = Mn/(Mn + Fe) and #Mn* = Mn*/(Mn* + Ca*). Further explanations in the text.

	Type 2	**Type 2**	**Type 2**	**Type 2**	**Type 2**	**Type 3**	**Type 3**	**Type 3**	**Type 4**
wt %	Sz29/2	Sz29/5	Sz29/13	Sz29/16	Sz29/25	Sz97/2	Sz94/141	Sz94/144	Sz132/4
$P_2O_{5(cal.)}$	40.42	39.53	39.81	38.87	40.41	40.71	40.27	40.08	39.00
As_2O_5	b.d.l.	b.d.l.	b.d.l.	b.d.l.	b.d.l.	b.d.l.	b.d.l.	b.d.l.	1.01
FeO	0.68	0.96	0.56	1.25	0.22	0.33	0.54	0.29	0.82
MnO	21.75	26.35	16.87	22.57	10.61	18.94	19.23	18.33	1.99
MgO	b.d.l.	b.d.l.	b.d.l.	b.d.l.	b.d.l.	b.d.l.	b.d.l.	b.d.l.	b.d.l.
CaO	34.89	29.84	39.17	31.80	45.04	38.22	37.47	38.74	52.51
SrO	b.d.l.	b.d.l.	b.d.l.	1.51	0.12	b.d.l.	b.d.l.	b.d.l.	0.22
Na_2O	b.d.l.	b.d.l.	b.d.l.	b.d.l.	0.04	b.d.l.	b.d.l.	b.d.l.	0.29
K_2O	b.d.l.	b.d.l.	b.d.l.	b.d.l.	b.d.l.	b.d.l.	b.d.l.	b.d.l.	b.d.l.
F_2	0.50	b.d.l.	0.56	b.d.l.	1.21	1.25	2.21	1.67	b.d.l.
Cl_2	2.61	3.52	2.28	4.58	1.98	0.14	b.d.l.	b.d.l.	4.35
$H_2O_{(cal.)}$	0.80	0.77	0.85	0.48	0.64	1.09	0.66	0.91	0.61
$-O=F_2$	−0.21	0.00	−0.24	0.00	−0.51	−0.53	−0.93	−0.70	0.00
$-O=Cl_2$	−0.59	−0.79	−0.51	−1.03	−0.45	−0.03	0.00	0.00	−0.98
Total	100.85	100.17	99.35	100.12	99.32	100.13	99.45	99.31	99.81
apfu									
$PO_4^{3-}{}_{(cal.)}$	3.01	3.02	2.99	2.99	2.99	3.00	3.00	2.98	2.89
AsO_4^{3-}									0.05
F^-	0.14		0.16		0.34	0.34	0.61	0.46	
Cl^-	0.39	0.54	0.34	0.71	0.29	0.02			0.64
$OH^-{}_{(cal.)}$	0.47	0.46	0.50	0.29	0.37	0.64	0.39	0.54	0.36
Ca^{2+}	3.29	2.88	3.72	3.10	4.22	3.57	3.53	3.65	4.92
Sr^{2+}				0.08	0.01				0.01
Mn^{2+}	1.62	2.01	1.27	1.74	0.79	1.40	1.43	1.35	0.15
Fe^{2+}	0.05	0.07	0.04	0.09	0.02	0.02	0.04	0.02	0.06
Mg^{2+}									
Na^+					0.01				0.05
K^+									
#Mn	0.97	0.97	0.97	0.95	0.98	0.98	0.97	0.99	0.71
#Mn*	0.34	0.42	0.26	0.37	0.16				
^{M1}Ca*	**1.87**	**1.49**	**1.99**	**1.92**	**2.02**				
^{M1}Mn*	0.09	0.47	0.04	0.09	0.02				
^{M2}Ca*	1.42	1.39	**1.73**	1.26	**2.21**				
^{M2}Mn*	**1.58**	**1.61**	1.27	**1.74**	0.79				

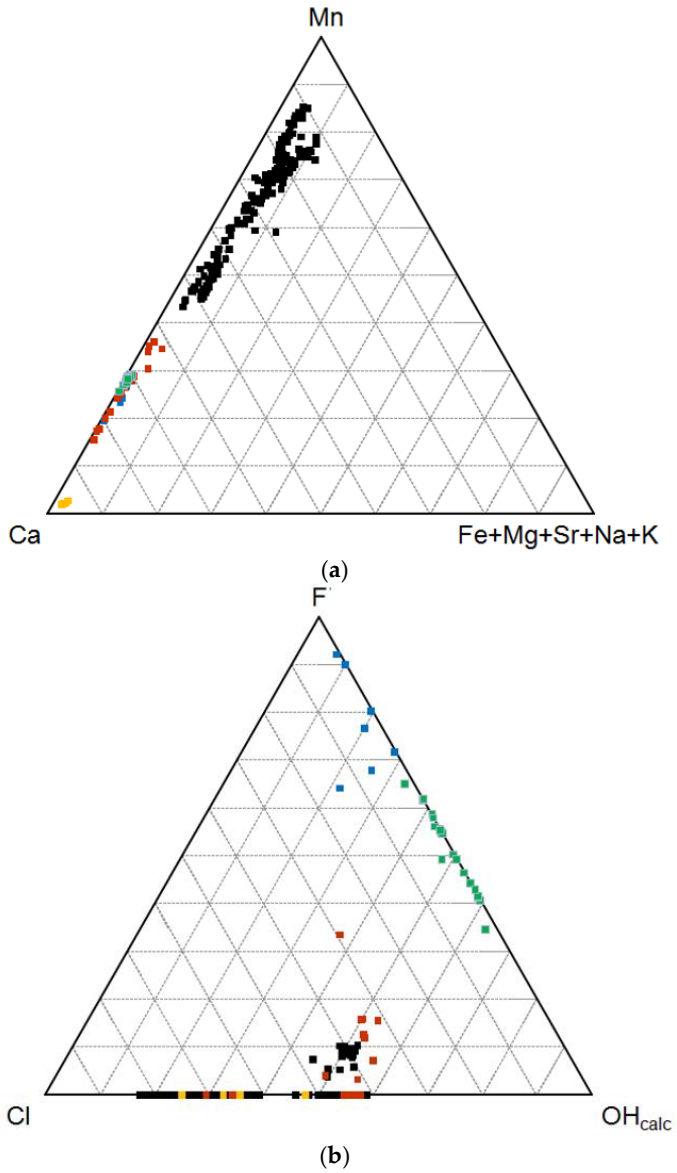

Figure 3. Chemical composition of Types 1–4 *apatites* from the Szklary pegmatite compared to *common apatite* from the same pegmatite (data from [8]) in the triangular diagrams: (**a**) Mn–Ca–∑(Fe + Mg + Sr + Na + K) and (**b**) F–Cl–OH_{cal}. Colours: black—Type 1, red—Type 2, green—Type 3, yellow—Type 4, blue—*common apatite*.

Type 2 is compositionally variable, reflecting the patchy zoning pattern. However, compared to Type 1, Type 2 *apatites* have much lower contents of MnO, ranging from 10.61 to 23.68 wt % (0.79–1.80 *apfu*) and higher contents of CaO from 31.80 to 45.04 wt % (3.10–4.22 *apfu*). They also contain less FeO (0.19–1.25 wt %, ≤0.09 Fe *apfu*). Trace amounts ≤1.61 wt % of SrO (≤0.08 *apfu*) and ≤0.04 wt % of Na_2O (≤0.01 *apfu*) are present while MgO and K_2O are below detection limits. In domains with higher concentrations of Mn the amounts of Cl can reach up to 4.58 wt % (0.71 *apfu*), although they decrease to 1.98 wt % (0.29 *apfu*) in Mn-poorer regions. Fluorine, up to 1.21 wt % F (≤0.34 *apfu*), is generally present in areas with lower Mn, and the calculated OH ranges from 0.29 to 0.58 *apfu*.

Type 3 *apatites* are rather homogeneous compositionally and in many respects resemble the compositions of *common apatites* (Figure 3). They have between 17.36 and 19.87 wt % MnO (1.29–1.46 *apfu*) and from 37.44 to 39.89 wt % CaO (3.49–3.71 *apfu*). The concentrations of FeO do not exceed 0.60 wt % (≤0.04 *apfu*) while MgO and Na_2O reach, respectively, 0.07 wt % and 0.04 wt %

(≤0.01 *apfu*). MgO and K_2O are below detection limits. A characteristic feature of this type of *apatites* is the general absence of Cl that only in rare cases reaches 0.20 wt % (≤0.03 *apfu*). In contrast to Type 1 and Type 2, the *X* site of Type 3 *apatites* is occupied mostly by 1.25–2.35 wt % F (0.34–0.65 *apfu*) and 0.34–0.63 OH *apfu*. On the other hand, Type 3 *apatites* show lower contents of F than *common apatites* (Figure 3b).

The variation of the Mn/(Mn + Fe) ratio (#Mn), an indicator of Mn–Fe geochemical fractionation, confirms the crystallization sequence inferred from textural observations and the high degree of Mn–Fe fractionation in the investigated mineral assemblages. In Type 1 the ratio varies from 0.84 to 0.98, although in a great majority of the analyses it is between 0.90 and 0.95. The lowest Mn–Fe fractionation is in the compositions with the highest contents of Fe and Mg. The #Mn values of Type 1 *apatites* partly overlap, or are higher than, the values of 0.74–0.88 in the associated beusites (Table 4). It may suggest that the Type 1 *apatites* crystallized simultaneously with or slightly later than the co-existing beusites. The #Mn values in the Type 2 *apatites* (0.95–0.98) are higher compared to Type 1 and slightly increase further in Type 3 *apatites* (0.97–0.99). In general, the fractionation index of Types 2,3 *apatites* approaches unity, partly overlaps with the highest values achieved by the Type 1, and roughly coincides with #Mn observed in the *common apatites*.

Table 4. Average compositions of beusites associated with Type 1 *apatites* from the Szklary pegmatite. The compositions of beusite-(Ca) from Sz108 sample due to its heterogeneity are presented as selected representative analyses. Abbreviations: Sz26/35 = sample/analysis, Beu—beusite, Cbeu—beusite-(Ca), #Mn = Mn/(Mn + Fe).

	Sz26	**Sz31**	**Sz94**	**Sz108/31**	**Sz108/39**	**Sz108/9**
wt %	Beu	Beu	Cbeu	Beu	Cbeu	Cbeu
$P_2O_{5(cal.)}$	41.19	41.83	41.28	41.09	41.11	41.27
FeO	7.59	12.47	6.07	11.69	11.81	10.94
MnO	43.82	38.77	44.88	38.17	34.95	33.79
MgO	0.89	2.24	0.37	1.14	0.89	0.93
CaO	6.91	5.63	8.20	7.95	10.77	12.45
Total	100.40	100.94	100.80	100.03	99.52	99.38
apfu						
$PO_4^{3-}{}_{(cal.)}$	2.00	2.01	2.00	2.00	2.00	2.00
Ca^{2+}	0.43	0.34	0.52	0.49	0.66	0.76
Mn^{2+}	2.13	1.86	2.18	1.86	1.70	1.64
Fe^{2+}	0.36	0.59	0.28	0.56	0.57	0.52
Mg^{2+}	0.08	0.19	0.03	0.10	0.07	0.08
#Mn	0.85	0.76	0.89	0.77	0.75	0.76

Type 4 *apatites* are geochemically different from Types 1–3 and show only 1.46–1.99 wt % MnO (0.11–0.15 *apfu*) at 51.67–53.91 wt % CaO (4.85–4.97 *apfu*). They also contain trace amounts 0.20–0.38 wt % of Na_2O (0.03–0.05 *apfu*), 0.40–0.82 wt % FeO (0.03–0.06 *apfu*) and, characteristically, also 0.09–0.34 wt % SrO (≤0.02 *apfu*). In contrast to the other investigated *apatites*, the analyses also show the presence of minor As substituting for P (0.99–2.06 wt % As_2O_5, 0.05–0.09 AsO_4^{3-} *apfu*). The *X* site is typically dominated by Cl (3.07–5.08 wt %; 0.45–0.75 *apfu*) and the calculated content of OH is 0.25–0.55 *apfu*. In one analytical point $OH_{cal.}$ is prevalent over Cl. The presence of F was not detected. Type 4 *apatites* show also moderate #Mn between 0.70 and 0.79, distinctly lower than in the other *apatites* from the Szklary pegmatite. However, #Mn in this type is rather controlled by the chemical composition of the xenolith and not by fractional crystallization of the pegmatite-forming minerals.

Figures 4 and 5 present correlations between the main chemical components and the dependence of the concentrations of these elements on the #Mn values, respectively. A nearly perfect negative correlation between Ca + Sr and Mn for all the investigated *apatites* and strong positive correlation between Cl and Mn coupled with a good negative correlation of Ca+Sr against Cl for Types 1,2 indicate that the compositional variation in Types 1,2 *apatites* is defined by a solid-solution between

end-members hydroxylapatite, $Ca_5(PO_4)_3OH$, and pieczkaite, $Mn_5(PO_4)_3Cl$. Types 3,4 *apatites* show different behaviour as concerns the dependence of Mn and Ca + Sr on the Cl content. Taking into account also the distribution of the analytical points in Figure 3, it seems that Type 3, nearly devoid of Cl, shows strong similarities to *common apatites* while the compositional variation of the Mn-poor Type 4 is confined to the chlorapatite-hydroxylapatite solid-solution. Negative correlations between Fe and Ca + Sr and between Fe and the extent of Mn–Fe fractionation suggest that the Mn–Fe fractionation in the crystallization environment of Types 1–3 *apatites* resulted from a decreasing Fe concentration, probably driven by precipitation of Fe-bearing minerals such as tourmaline, garnet and *biotite*. Other elements do not show any clear dependence on the #Mn value. However, generally, the transition from the precipitation of Type 1 to the subsequent Types 2,3 that takes place at #Mn near 0.96 is marked by a decrease of the Mn activity coupled to an increase in the role of Ca in the *apatites* structure. Similarly, the role of Cl at the *X* site diminishes and the content of F rises towards (though not attaining) the amounts observed in the *common apatites*.

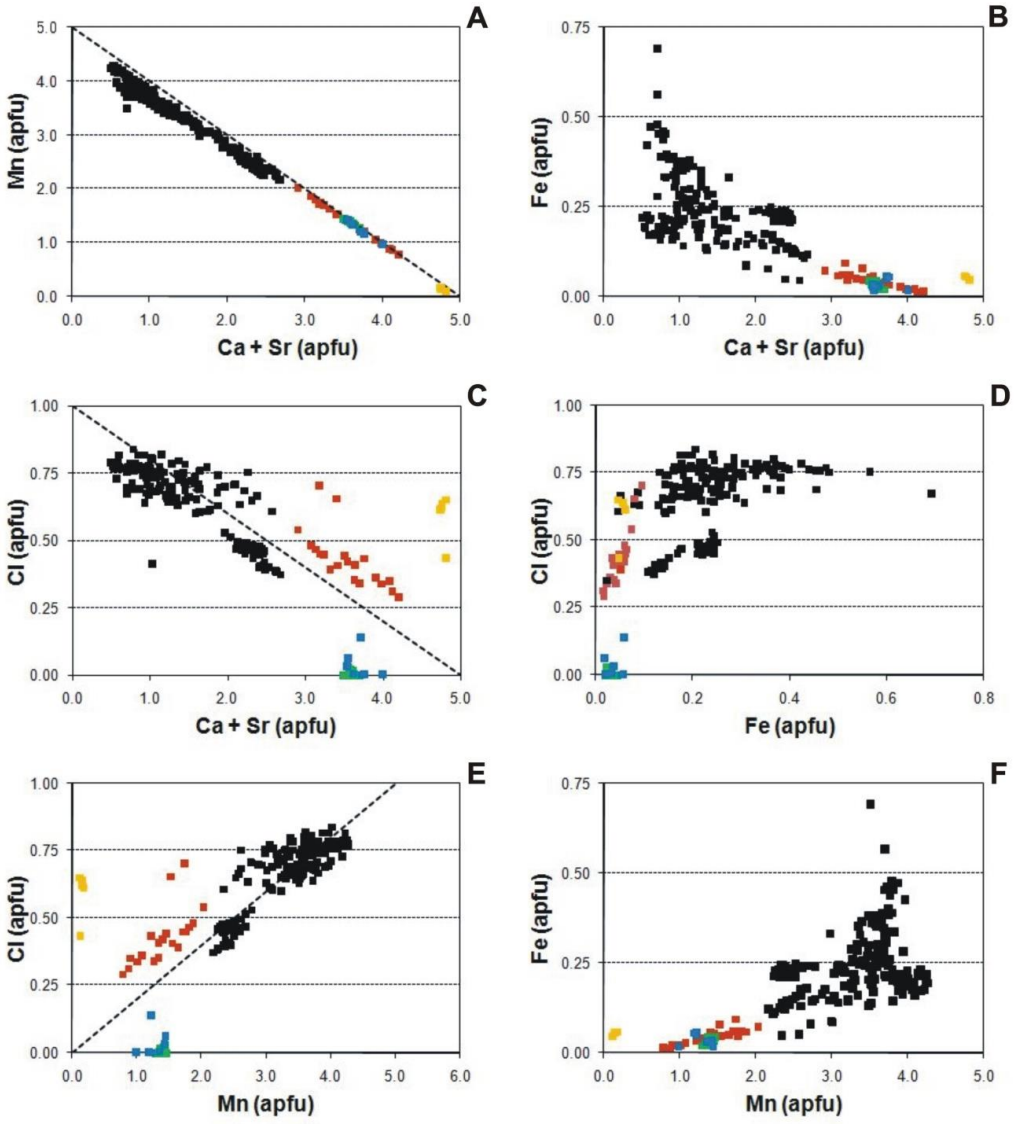

Figure 4. Correlations Ca + Sr vs. Mn (**A**), Ca+Sr vs. Fe (**B**), Ca+Sr vs. Cl (**C**), Fe vs. Cl (**D**), Mn vs. Cl (**E**), and Mn vs. Fe (**F**) in the structure of *apatites* from the Szklary pegmatite. Colours as in Figure 3, dashed line: ideal trend in the pieczkaite–hydroxylapatite solid solution, $Mn_5(PO_4)_3Cl$–$Ca_5(PO_4)_3OH$.

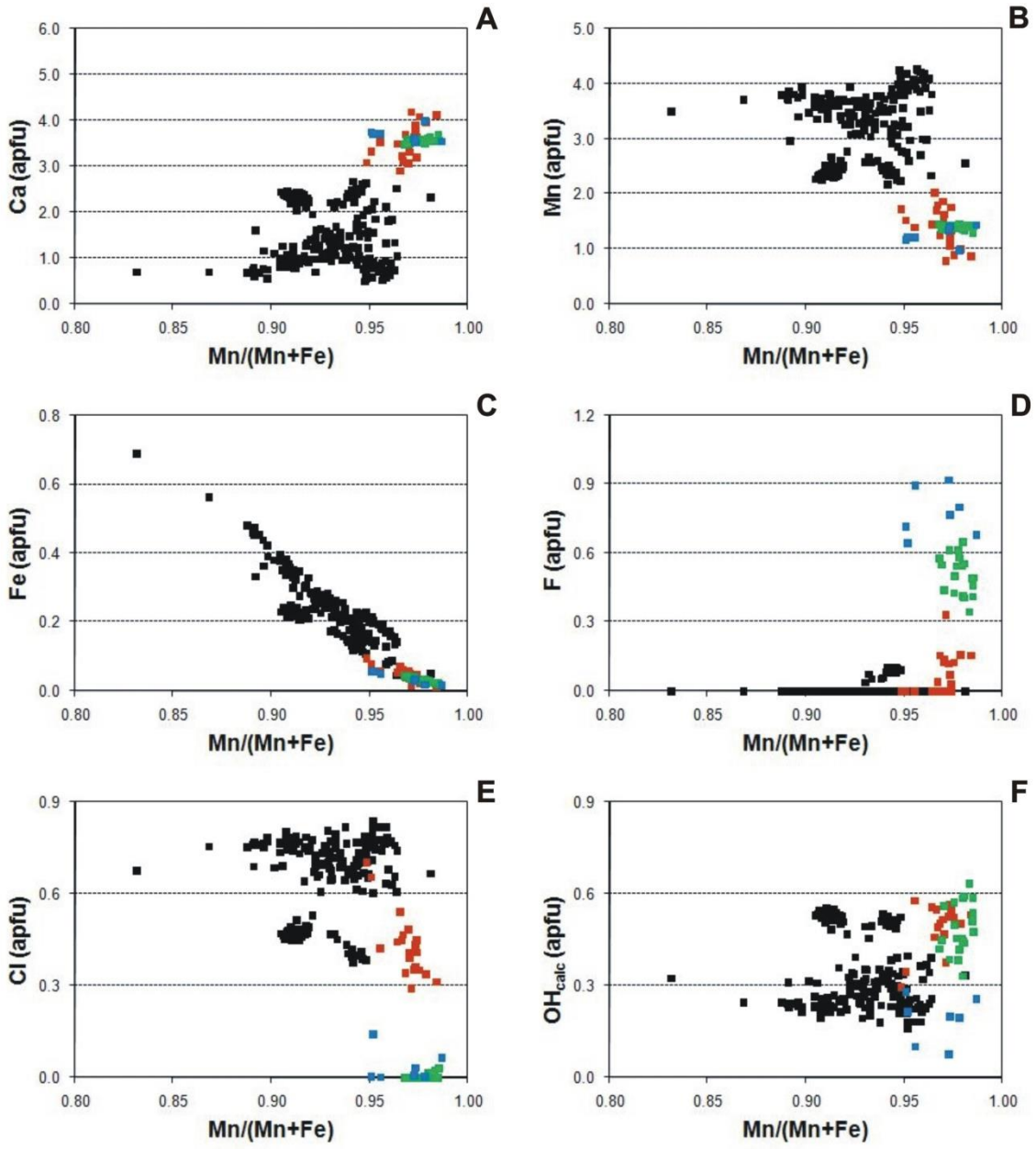

Figure 5. Dependences of Ca (**A**), Mn (**B**), Fe (**C**), F (**D**), Cl (**E**) and OH_{calc} (**F**) on the Mn/(Mn + Fe) fractionation index in the structure of *apatites* from the Szklary pegmatite. Colours as in Figure 3. Type 4 *apatites* are out of scale of the figures with significantly lower values of Mn/(Mn + Fe).

6. Taxonomic Implications

Relating Type 3 and Type 4 *apatites* to the current classification scheme is straightforward and the two distinct groups represent Mn-rich hydroxyl- to fluorapatite and chlorapatite, respectively. However, classification of the Type 1 and Type 2 compositions, the primary target of this study, is more challenging. A large number of the analyses of Types 1,2 show Mn > 2.5 *apfu* and Cl > 0.5 *apfu* (Tables 2 and 3) and, therefore, correspond to pieczkaite. However, among the Types 1,2 compositions there are also analyses with Mn < 2.5 *apfu* and Cl close to 0.5 *apfu* (Sz31 and Sz79; Table 2) or even below that threshold value (Sz 29; Table 3). Negligible fluorine contents and the correlations between chemical components discussed above (Figure 4) suggest that these analyses represent intermediate compositions between the end-member pieczkaite, $Mn_5(PO_4)_3Cl$, and hydroxylapatite, $Ca_5(PO_4)_3OH$, with a dominance of the latter component. If no significant Ca–Mn ordering between the *M*1 and *M*2

structural sites takes place, these compositions would correspond to extremely Mn-rich hydroxylapatite. However, the taxonomy becomes far more complex if ordering of Ca and Mn is to be taken into account. It has been demonstrated for pieczkaite and Mn-rich fluorapatite that Mn preferentially enters the *M*2 site if the *X* site is dominated by Cl, the *M*1 site being favoured if the *X* site is occupied predominantly by F [4,5,7,42]. Although, to our knowledge, no systematic research has been carried out on the Ca–Mn ordering in the apatite-group minerals with the *X* site dominated by OH, Tait et al. [7] observed that Ca is locally associated with OH at the neighbouring *X* sites and that the *X*-site anion is bonded to three *M*2 sites in the structure of the Cross Lake pieczkaite. Therefore, at negligible fluorine content, two potential intermediate species with fully ordered compositions may be postulated: $Ca_2Mn_3(PO_4)_3$(Cl > OH) and $Mn_2Ca_3(PO_4)_3$(Cl < OH), formally $Ca_2Mn_3(PO_4)_3Cl$ and $Mn_2Ca_3(PO_4)_3OH$, respectively. Of particular interest is that these hypothetical end-members have different prevailing cations at the *M*1 and *M*2 sites and, according to the current nomenclature scheme [1], should classify not into the apatite group (together with pieczkaite and hydroxylapatite) but into the hedyphane group within the apatite supergroup.

In order to discuss the probable classification of Types 1,2 *apatites* from Szklary with the assumption of maximum Ca–Mn ordering, and taking into account both hypothetical end-members, it is useful to consider the calculated formulae in terms of Ca* = Ca + Sr + Na + K and Mn* = Mn + Fe + Mg. Hypothetical allocations of Ca* and Mn* between the *M*1 and *M*2 sites for representative compositions of Types 1,2 *apatites* are presented in Tables 2 and 3. The maximum amount of ^{M2}Ca* is calculated from ^{M2}Ca* = 3·OH *pfu* and the remaining Ca* constitutes the minimum amount of ^{M1}Ca*. If Ca* < 3 OH, all Ca* fills the *M*2 site. In this approach, the analyses with pieczkaite stoichiometry have #Mn* (Mn*/(Mn* + Ca*)) from 0.55 to 0.90 and the Cl content in the range of 0.46–0.83 *apfu* (Table 2). The compositions corresponding to $Ca_2Mn_3(PO_4)_3Cl$ have #Mn* in the range 0.48–0.65 and the *X*-site dominated by Cl (0.40–0.77 *apfu*). The compositions approaching $Mn_2Ca_3(PO_4)_3(OH)$ have #Mn* between 0.49 and 0.53, and Cl contents in the range 0.40–0.46 *apfu*. Compositions with #Mn* $\leq$ 0.47 and Cl $\leq$ 0.39 *apfu* have both cation positions dominated by Ca* and represent more or less Mn-rich hydroxylapatite.

The analyses of Type 1 are pieczkaite with the two grains built mostly of $Ca_2Mn_3(PO_4)_3Cl$ (sample Sz31) and $Mn_2Ca_3(PO_4)_3(OH)$ (sample Sz79). In sample Sz79, single analytical points represent pieczkaite or highly Mn-rich hydroxylapatite. The analyses of Type 2 *apatites* correspond mostly to highly Mn-rich hydroxylapatite with some compositions showing $Ca_2Mn_3(PO_4)_3Cl$ stoichiometry. There are three analyses of Type 2 *apatite* (sample Sz29) that correspond to $Ca_2Mn_3(PO_4)_3Cl$ (all with Cl > OH and #Mn* $\leq$ 0.37). All the remaining analyses in this sample correspond to the hydroxylapatite–pieczkaite solid solution with the *M*1 and *M*2 sites dominated by Ca (#Mn* $\leq$ 0.36) and OH slightly prevalent over Cl in the *X* site.

It must also be stressed that an alternative approach to the problem of cation ordering in Mn-rich *apatites* with the *X* site populated by Cl and OH is also possible, in which the degree of ordering depends on the amount of the *M*2 sites coordinated by Cl. In this approach, certain amount of Mn enters preferentially only these *M*2 positions that are coordinated by Cl but this mechanism does not operate for the *M*2 positions coordinated by OH. In this case, it is only possible to achieve partial Mn–Ca ordering and compositions of such *apatites* could be described by solid solutions between the end-members of hydroxylapatite, $Ca_5(PO_4)_3(OH)$, chlorapatite $Ca_5(PO_4)_3Cl$, and pieczkaite, $Mn_5(PO_4)_3Cl$, all classifying to the apatite-group.

Therefore, possible allocations of Mn and Ca between the cationic sites of the fully ordered apatite structure should be verified by detailed structural studies. Such studies are needed in order to elucidate the extent of Mn ordering in the solid-solution series $(Mn,Ca)_2(Mn,Ca)_3(PO_4)_3(Cl,OH)$ and to verify the status of the hypothetical $Ca_2Mn_3(PO_4)_3Cl$ and $Mn_2Ca_3(PO_4)_3OH$ phases.

7. Genetic Implications

In order to discuss the origin of the Cl- and Mn-rich *apatites* from Szklary, the following issues are of primary importance: (1) the stage of pegmatite formation at which these minerals crystallized, (2) processes responsible for creating the environment unusually rich in Mn and Cl, and (3) possible sources of Cl and Mn. In the Cross Lake pegmatite, the type locality for pieczkaite, early crystallized Mn-rich fluorapatite is succeeded by late Mn-rich chlorapatite and pieczkaite [7]. This mineral sequence, along with the presence of unusually Mn-rich assemblage of other phosphates with bobfergusonite and manitobaite [43,44], record the build-up of Mn and F and later also of Cl concentrations with the progress of pegmatite crystallization. This is consistent with the general observation that high contents of OH + Cl, and particularly the Cl-enrichment in the apatite structure, are characteristic of late to secondary stages of pegmatitic evolution or of a low-temperature hydrothermal environment [45,46]. The holotypic Cross Lake pieczkaite formed from highly evolved late-stage residual fluids that could have become additionally enriched in Mn–Cl complexes by reacting with earlier-crystallized minerals [7]. The Szklary pegmatite resembles in many respects the pieczkaite-bearing Cross Lake pegmatite, i.e.,: (i) it is also highly evolved, (ii) it shows unusually high Mn/(Mn + Fe) ratios and contains a similar assemblage of Mn-phosphates, (iii) there is plenty of evidence for the late-stage residual fluids back-reacting with earlier crystallized phases [8,35], some of which (e.g., micas and Mn-bearing cordierite) might be considered as a potential source for Mn and Cl. Therefore, Pieczka [7] generally followed a similar line of reasoning although he suggested that the enrichment of the pegmatite-forming melt in Cl might already have taken place in the source. He proposed also that the initial high amount of Mn increased solubility of Cl in the melt that was later reduced by crystallization of minerals rich in Ca, Mg, Fe, Al, P, and F, such as tourmaline, beusites, and Mn-rich fluorapatite. The decrease in the solubility of Cl is supposed to have resulted in the exsolution of a late-stage Cl- and Mn-rich fluid or highly fluxed melt. Such a medium could have reacted with earlier crystallized Mn-bearing phosphates, increasing the concentrations of Mn even further and creating the conditions favourable for the formation of *apatites* unusually enriched in Mn and Cl.

However, the current studies have shown that, contrary to the Cross Lake pieczkaite, the Cl- and Mn-rich *apatites* of Types 1,2 from Szklary are primary magmatic phases that formed together with, and possibly also slightly after *beusites*. Their crystallization predated Mn-rich fluor- and hydroxylapatites. Therefore, simple scenarios relating the crystallization of pieczkaite and the other Cl- and Mn-rich *apatites* from Szklary to late-stage Mn- and Cl-enriched residual fluids are not satisfactory. It rather seems that the crystallization of the assemblage of pieczkaite (Type 1 *apatites* of this study) ± beusite marks a short-lived magmatic episode of precipitation from the hydrous melt extremely enriched in Mn, Cl, and P. This episode seems to be an anomaly in the overall evolution of the Szklary pegmatite, as suggested by the fact that these minerals occur as rare accessories only locally in the intermediate graphic zones (2) and (3). The assemblage of the Type 1 *apatites* ± beusite in the beryl–columbite–phosphate Szklary pegmatite might be treated in many respects as a counterpart of polymineral nodular segregations of primary magmatic Fe–Mn phosphates such as graftonites, beusites, triphylite, and sarcopside known from P-enriched GSB pegmatites, cogenetic with the Szklary pegmatite [39,47,48]. Phosphate mineralization in the Lutomia pegmatite, one of these GSB P-enriched bodies, has been investigated in detail [47]. The authors followed the concept that separation of two geochemically distinct melts due to melt-melt immiscibility may play an important role in the evolution of a pegmatite (e.g., [49–52]). Włodek et al. [47] proposed that the phosphate nodules at Lutomia crystallized from a P-rich melt which unmixed from the aluminosilicate melt upon cooling.

All things considered, we propose that the assemblage of the Type 1 *apatites* ± beusite in the Szklary pegmatite may be a product of crystallization from small-volume droplets of melt rich in Mn, Cl and P unmixed from its "normal" aluminosilicate counterpart. Whether the unmixing is a pre-, syn-, or post-emplacement process remains an open question. The enrichment in Cl of the P-rich melt relative to the "normal" melt might be a result of the preferential partitioning of this element into the unmixed

droplets. The P-rich melt with a high content of Cl could have been additionally enriched in Mn due to chloride complexing and effective scavenging of available Mn from the surrounding "normal" melt. Small volumes of such an unmixed melt could be responsible for the "episodic" and local character of such crystallization events. In such a scenario, the Type 2 *apatites* with disequilibrium patchy texture can be interpreted as a product of the waning stage of this episode. At that stage, the crystallization took place at the presence of two conjugate highly fluxed melts: the residual portions of P-rich melt already impoverished but still enriched in Mn and Cl and the "normal" pegmatitic melt that induced the formation of domains of Mn-rich hydroxylapatite with Ca > Mn and OH + F dominating over Cl. At that stage, there is a noticeable tendency for decreasing concentrations of Cl and increasing OH and F coupled to a decreasing role for Mn with the progress in crystallization. The Type 3 *apatites*, crystallized from the "normal" pegmatitic melt, probably after the droplets of P-rich melt had been entirely consumed. They differ from the *normal apatites* only in slightly lower contents of F but the two groups represent the Mn-enriched fluorapatite–hydroxylapatite solid solution, nearly completely devoid of Cl.

Compared to other pegmatites related to the anatectic event in the GSB geological unit, the Szklary pegmatite is distinguished by the large extent of Mn–Fe fractionation observed already at a relatively early stage of crystallization. This is manifested by high concentrations of Mn in cordierite with up to 25% of hypothetical Mn-cordierite [53], high values of Mn/(Mn + Fe) ranging from 0.72 to 0.87 in the columbite-group minerals and highly manganoan compositions of garnet with over 80% of the spessartine molecule [33,35]. The serpentinites of the Szklary massif that host the pegmatite contain too low concentrations of Mn, generally below 0.12 wt % MnO [54], to regard them as a likely source for in situ Mn contamination. This is also shown by the low contents of Mn in Type 4 *apatites* that formed next to the digested serpentinite xenolith. On the other hand, our present knowledge on the mineralogy of the pegmatite does not warrant serious consideration of in situ fractional crystallization as a mechanism responsible for the observed high extent of Mn–Fe fractionation. Therefore, the enrichment of the melt in Mn relative to Fe must have taken place before emplacement. It could have been acquired directly at the melt's source, especially if the source rocks contained for instance Mn-rich ocean-floor sediments—not an unlikely scenario in the accretionary complex of the Central Sudetes. Other possible scenarios include pre-emplacement fractional crystallization followed by separation of the evolved melt from the restitic phases with low Mn/(Mn + Fe) or the contamination of the ascending melt by Mn-enriched rocks. On the other hand, high concentrations of Cl in Type 4 *apatites* near the serpentinite xenolith suggest that local enrichment of the pegmatite-forming melt in Cl is a result of contamination by host rocks. Although the data on the concentration of Cl in the Szklary serpentinites is lacking, the sea-floor serpentinites and associated metasediments typically contain significant amounts of Cl that might be released, recycled and locally concentrated in supra-subduction zones (e.g., [55–58]). It is noteworthy that the Szklary pegmatite is the only known example of a GSB pegmatite emplaced outside the crustal-related GSB geological unit into the geochemically contrasted ophiolitic rock suite of the Szklary Massif. This fact may explain the high content of Cl compared to other GSB pegmatites. Some metasomatic interaction between the Szklary pegmatite and serpentinite wall rocks took place as indicated by vermiculite–talc–chlorite zone present along the pegmatite–serpentinite contact. Therefore, circulation of chemically aggressive hydrothermal fluids, driven by heat from the cooling pegmatite, could be also responsible for leaching some Cl from the serpentinites and adding this halogen to the pegmatite at the hydrothermal stage of evolution. This process could have been responsible for the late-stage hydrothermal alteration of some of the *common apatites* that developed mainly along fractures in the crystals as Cl-enriched Mn-poor secondary domains [8]. However, the small size of the Szklary pegmatite and, consequently, the small volume of the convecting orthomagmatic fluid derived from the pegmatite-forming melt suggest a rather low efficiency for this process. Besides, the crystallization of the *apatites* of Types 1,2, the primary target of this study, took place at the magmatic stage and cannot be related to crystallization from the late-stage hydrothermal fluids. The estimation of percentage of Cl

in the pegmatite that was added from external source through wall rock assimilation is not possible at this stage of our studies and would require isotopic investigations.

It should also be stressed that younger intrusions of dioritic, syenitic, and granodioritic magmas at ~335–340 Ma that took place in the Niemcza Shear Zone could have generated hydrothermal fluids that induced metasomatic alteration of the Szklary pegmatite mineral assemblages. However, the present state of knowledge does not permit us to estimate the extent of such alteration.

8. Conclusions

The Szklary pegmatite is, to our knowledge, the second occurrence of pieczkaite worldwide. *Apatites* from Szklary that approach or attain the stoichiometry of pieczkaite (Types 1,2 *apatites* of this study) have compositions defined by two independent substitutions of Mn for Ca and Cl for OH. If no ordering of Ca and Mn between the cationic sites takes place, they represent the Mn-rich sector of the solid solution $^{M1}(Mn,Ca)_2{}^{M2}(Mn,Ca)_3(PO_4)_3{}^{X}(Cl,OH)$ and vary from extremely Mn-rich hydroxylapatite to pieczkaite, $^{M1}Mn_2{}^{M2}Mn_3(PO_4)_3{}^{X}Cl$. However, if the maximum Mn–Ca ordering is assumed (and following the observations that Mn prefers the *M*2 site if the *X* site is dominated by Cl and the *M*1 site is favoured if the *X* site is dominated by OH), apart from the compositions that represent pieczkaite and Mn-rich hydroxylapatite, there are intermediate compositions for which the existence of two hypothetical end-member species can be postulated: $^{M1}Ca_2{}^{M2}Mn_3(PO_4)_3{}^{X}Cl$ and $^{M1}Mn_2{}^{M2}Ca_3(PO_4)_3{}^{X}OH$. It is noteworthy that these hypothetical species would classify into the hedyphane group within the apatite supergroup while hydroxylapatite and pieczkaite are members of the apatite-group in the current classification of the apatite supergroup. Alternatively, it can be assumed that Mn enters preferentially only these *M*2 positions that are coordinated by Cl but this mechanism does not operate for the *M*2 positions coordinated by OH. In that case, only partial Mn-Ca ordering in such *apatites* would be possible.

In contrast with the type locality at Cross Lake (Manitoba, Canada), where pieczkaite formed from highly evolved late-stage residual fluids [7], the pieczkaite-like *apatites* from Szklary (Types 1,2 *apatites*) crystallized rather in a short-lived magmatic episode, together or slightly after *beusites*, from a hydrous melt extremely enriched in Mn, Cl, and P before Mn-rich hydroxyl- (Type 2 *apatites*) and fluorapatites (Type3 *apatites*). During crystallization of the assemblage of *beusites* and Types 1–3 *apatites*, the activities of Mn and Cl decreased whereas the role of Ca and F increased. Another group of atypical *apatites* (Type 4) from Szklary represent Mn-poor chlorapatite and document local wall rock contamination. We propose that *apatites* (Types 1,2) with pieczkaite-like compositions in the Szklary pegmatite formed from small-volume droplets of P-rich melt that unmixed from the LCT pegmatite-forming melt, which already upon emplacement had a high Mn/(Mn + Fe) ratio and became locally enriched in Cl through in situ contamination by wall rock serpentinites. The specific geotectonic setting of the pegmatite, at the boundary between crustal-related and ocean-related geological units in the Central Sudetic accretionary complex, is a critical factor involved in creating the favourable geochemical environment for a combination of metasedimentary rock series as a melt source and ocean-related lithologies as a contaminant. However, the extent of wall rock contamination and the hypothetical influence of hydrothermal reworking related to a younger magmatic event at ~335–340 Ma require further studies.

Author Contributions: A.S. wrote the text, prepared most of the figures and suggested the genetic model of the mineralization; A.P. and B.G. supplied the samples, performed and recalculated the EPMA analyses; M.M. and M.D.-S. performed the SEM studies; E.S. prepared some figures and contributed to the discussion on the mineralization origin.

Funding: The research was founded by the National Science Centre (Poland) grant number 2015/17/B/ST10/03231 and the University of Wroclaw grant 0401/0156/18.

Acknowledgments: We thank the anonymous Reviewers and the Editor for their insightful comments and helpful suggestions. We also acknowledge Ray Macdonald's help in language corrections.

Conflicts of Interest: The authors declare no conflict of interest. The founding sponsors had no role in the design of the study; in the collection, analyses, or interpretation of data; in the writing of the manuscript, and in the decision to publish the results.

References

1. Pasero, M.; Kampf, A.R.; Ferraris, C.; Pekov, I.V.; Rakovan, J.; White, T.J. Nomenclature of the apatite supergroup minerals. *Eur. J. Mineral.* **2010**, *22*, 163–179. [CrossRef]
2. Hughes, J.M.; Rakovan, J. Structurally robust, chemically diverse: Apatite and apatite supergroup minerals. *Elements* **2015**, *11*, 167–172. [CrossRef]
3. Hughes, J.M.; Harlov, D.; Kelly, S.R.; Rakovan, J.; Wilke, M. Solid-solution in the apatite OH–Cl binary system. Compositional dependence of solid-solution mechanisms in calcium phosphate apatites along the Cl–OH binary. *Am. Mineral.* **2016**, *101*, 1783–1791. [CrossRef]
4. Hughes, J.M.; Cameron, M.; Crowley, K.D. Ordering of Divalent Cations in the Apatite Structure: Crystal Structure Refinements of Natural Mn- and Sr-Bearing Apatite. *Am. Mineral.* **1991**, *76*, 1857–1862. Available online: http://www.minsocam.org/ammin/AM76/AM76_1857.pdf (accessed on 17 January 2018).
5. Hughes, J.M.; Ertl, A.; Bernhardt, H.J.; Rossman, G.R.; Rakovan, J. Mn-rich fluorapatite from Austria: Crystal structure, chemical analysis and spectroscopic investigation. *Am. Mineral.* **2004**, *89*, 629–632. [CrossRef]
6. Tait, K.T.; Hawthorne, F.C.; Černý, P. Minerals from the Cross Lake pegmatite, Manitoba, Canada. 5th International Symposium on Granitic Pegmatites, PEG 2011, Mendoza, Argentina. Conference Papers. *Asociación Geologica Argentina, Serie D, Publicación Especial* **2011**, *14*, 213–215. Available online: www.minsocam.org/msa/Special/Pig/PIG_Articles/PEG2011_Contributions.pdf (accessed on 17 January 2018).
7. Tait, K.; Ball, N.A.; Hawthorne, F.C. Pieczkaite, ideally $Mn_5(PO_4)_3Cl$, a new apatite-supergroup mineral from Cross Lake, Manitoba, Canada: Description and crystal structure. *Am. Mineral.* **2015**, *100*, 1047–1052. [CrossRef]
8. Pieczka, A. Beusite and unusual Mn-rich apatite from the Szklary granitic pegmatite, Lower Silesia, Poland. *Can. Mineral.* **2007**, *45*, 901–914. [CrossRef]
9. Chopin, F.; Schulmann, K.; Skrzypek, E.; Lehmann, J.; Dujardin, J.R.; Martelat, J.E.; Lexa, O.; Corsini, M.; Edel, J.B.; Štípská, P.; et al. Crustal influx, indentation, ductile thinning and gravity redistribution in a continental wedge: Building a Moldanubian mantled gneiss dome with underthrust Saxothuringian material (European Variscan belt). *Tectonics* **2012**, *31*, TC1013. [CrossRef]
10. Mazur, S.; Turniak, K.; Szczepański, J.; McNaughton, N.J. Vestiges of Saxothuringian crust in the Central Sudetes, Bohemian Massif: Zircon evidence of a recycled subducted slab provenance. *Gondwana Res.* **2015**, *27*, 825–839. [CrossRef]
11. Kryza, R.; Fanning, C.M. Devonian deep-crustal metamorphism and exhumation in the Variscan Orogen: Evidence from SHRIMP zircon ages from the HT–HP granulites and migmatites of the Góry Sowie (Polish Sudetes). *Geodin. Acta* **2007**, *20*, 159–176. [CrossRef]
12. Kryza, R. Migmatization in Gneisses of the Northern Part of the Sowie Góry, Sudetes. *Geol. Sudet.* **1981**, *16*, 7–91. Available online: https://geojournals.pgi.gov.pl/gs/article/view/25536/17405 (accessed on 17 January 2018). (In Polish)
13. Van Breemen, O.; Bowes, D.R.; Aftalion, M.; Żelaźniewicz, A. Devonian tectonothermal activity in the Sowie Góry gneissic block, Sudetes, southwestern Poland: Evidence from Rb-Sr and U-Pb isotopic studies. *J. Pol. Geol. Soc.* **1988**, *58*, 3–10.
14. Timmermann, H.; Parrish, R.R.; Noble, S.R.; Kryza, R. New U–Pb monazite and zircon data from the Sudetes Mountains in SW Poland: Evidence for a single-cycle Variscan orogeny. *J. Geol. Soc. Lond.* **2000**, *157*, 265–268. [CrossRef]
15. Turniak, K.; Pieczka, A.; Kennedy, A.K.; Szełęg, E.; Ilnicki, S.; Nejbert, K.; Szuszkiewicz, A. Crystallization age of the Julianna pegmatite system (Góry Sowie Block, NE margin of the Bohemian massif): Evidence from U-Th-Pb SHRIMP monazite and CHIME uraninite studies. In Proceedings of the 7th International Symposium on Granitic Pegmatites PEG 2015, Książ, Poland, 17–19 June 2015; Adam, S., Jan, C., Eds.; Book of Abstracts. Tigris: Zlín, Czech Republic, 2015; pp. 111–112.
16. Majerowicz, A.; Pin, C. Preliminary trace element evidence for an oceanic depleted mantle origin of the Ślęża ophiolitic complex, SW Poland. *Mineral. Pol.* **1986**, *17*, 3–22.

17. Oliver, G.J.H.; Corfu, F.; Krogh, T.E. U–Pb ages from SW Poland: Evidence for a Caledonian suture zone between Baltica and Gondwana. *J. Geol. Soc. Lond.* **1993**, *150*, 355–369. [CrossRef]
18. Dubińska, E.; Bylina, P.; Kozłowski, A.; Dörr, W.; Nejbert, K.; Schastok, J.; Kulicki, C. U–Pb dating of serpentinization: Hydrothermal zircon from a metasomatic rodingite shell (Sudetic ophiolite, SW Poland). *Chem. Geol.* **2004**, *203*, 183–203. [CrossRef]
19. Kryza, R.; Pin, C. The Central–Sudetic ophiolites (SW Poland): Petrogenetic issues, geochronology and palaeotectonic implications. *Gondwana Res.* **2010**, *17*, 292–305. [CrossRef]
20. Znosko, J. The problem of the oceanic crust and of ophiolites in the Sudetes. *Bull. Pol. Acad. Sci. Earth Sci.* **1981**, *29*, 185–197.
21. Matte, P.; Maluski, H.; Reilich, P.; Franke, W. Terrane boundaries in the Bohemian Massif: Results of large scale Variscan shearing. *Tectonophysics* **1990**, *177*, 151–170. [CrossRef]
22. Cymerman, Z.; Piasecki, M.A.J. The Terrane Concept in the Sudetes, Bohemian Massif. *Geol. Q.* **1994**, *38*, 191–210. Available online: http://www.jgeosci.org/detail/JCGS.814 (accessed on 1 February 2018).
23. Aleksandrowski, P.; Mazur, S. Collage tectonics in the northeasternmost part of the Variscan belt: The Sudetes, Bohemian massif. *Geol. Soc. Lond. Spec. Publ.* **2002**, *201*, 237–277. [CrossRef]
24. Żelaźniewicz, A. Deformation and metamorphism in the Góry Sowie gneiss complex, Sudetes, SW Poland. *Neues Jahrb. Geol. Palaeontol. Abh.* **1990**, *179*, 129–157.
25. Niśkiewicz, J. Geological structure of the Szklary Massif (Lower Silesia). *Ann. Soc. Géol. Pol.* **1967**, *37*, 387–417, (In Polish with English Summary).
26. Dubińska, E. Rodingites and amphibolites from the serpentinites surrounding Sowie Góry block (Lower Silesia, Poland): Record of supra-subduction zone magmatism and serpentinization. *Neues Jahrb. Mineral. Abh.* **1997**, *171*, 239–279.
27. Gunia, P. The Petrology and Geochemistry of Mantle-Derived Basic and Ultrabasic Rocks from the Szklary Massif in the Fore-Sudetic Block (SW Poland). *Geol. Sudet.* **2000**, *33*, 71–83. Available online: http://gs.ing.pan.pl/33_PDF/GS33_071-083.pdf (accessed on 17 January 2018).
28. Gunia, P. Plagiogranites from the Szklary Serpentinite Massif, a Component of the Sudetic Ophiolite. In Granitoids in Poland. Kozłowski, A., Wiszniewska, J., Eds. *Arch. Miner. Monogr.* **2007**, *1*, 287–295. Available online: http://geopark.org.pl/Badania/Gunia_Plagiogranites.pdf (accessed on 17 January 2018).
29. Pietranik, A.; Storey, C.; Kierczak, J. The Niemcza diorites and monzodiorites (Sudetes, SW Poland): A record of changing geotectonic setting at ca. 340 Ma. *Geol. Q.* **2013**, *57*, 325–334. [CrossRef]
30. Michalik, R. Gold in Serpentinite Weathering Cover of the Szklary Massif, Fore-Sudetic Block, SW Poland. *Geol. Sudet.* **2000**, *33*, 12–22. Available online: https://geojournals.pgi.gov.pl/gs/article/view/13800/12242 (accessed on 14 April 2018).
31. Černý, P.; Ercit, T.S. The classification of granitic pegmatites revisited. *Can. Mineral.* **2005**, *43*, 2005–2026. [CrossRef]
32. Černý, P.; London, D.; Novák, M. Granitic Pegmatites as Reflections of Their Sources. *Elements* **2012**, *8*, 289–294. Available online: http://www.jgeosci.org/10.2113/gselements.8.4.289 (accessed on 14 April 2018). [CrossRef]
33. Pieczka, A. A Rare Mineral-Bearing Pegmatite from Szklary Serpentinite Massif, the Fore-Sudetic Block, SW Poland. *Geol. Sudet.* **2000**, *33*, 23–31. Available online: https://geojournals.pgi.gov.pl/gs/article/view/13792/12234 (accessed on 17 January 2018).
34. Pieczka, A.; Szuszkiewicz, A.; Szełęg, E.; Janeczek, J.; Nejbert, K. Granitic pegmatites of the Polish part of the Sudetes (NE Bohemian massif, SW Poland). In *Fieldtrip Guidebook, Proceedings of the 7th International Symposium on Granitic Pegmatites PEG 2015, Książ, Poland, 17–19 June 2015*; Petr, G., Milan, N., Adam, S., Jan, C., Eds.; Tigris: Zlín, Czech Republic, 2015; pp. 73–103.
35. Pieczka, A. Primary Nb-Ta minerals in the Szklary pegmatite, Poland: New insights into controls of crystal chemistry and crystallization sequences. *Am. Mineral.* **2010**, *95*, 1478–1492. [CrossRef]
36. Pieczka, A.; Grew, E.S.; Groat, L.A.; Evans, R.J. Holtite and dumortierite from the Szklary pegmatite, Lower Silesia, Poland. *Mineral. Mag.* **2011**, *75*, 303–315. [CrossRef]
37. Pieczka, A.; Evans, R.J.; Grew, E.S.; Groat, L.A.; Ma, C.; Rossman, G.R. The dumortierite supergroup. II. Three new minerals from the Szklary pegmatite, SW Poland: Nioboholtite, $(Nb_{0.6}\square_{0.4})Al_6BSi_3O_{18}$, titanoholtite, $(Ti_{0.75}\square_{0.25})Al_6BSi_3O_{18}$, and szklaryite, $\square Al_6BAs^{3+}{}_3O_{15}$. *Mineral. Mag.* **2013**, *77*, 2841–2856. [CrossRef]

38. Pieczka, A.; Gołębiowska, B.; Szuszkiewicz, A.; Szełęg, E.; Szuszkiewicz, A. Bobfergusonite from the Szklary pegmatite, Poland, and its relation to other bobfergusonites. In Proceedings of the 8th International Symposium on Granitic Pegmatites PEG 2017, Kristiansand, Norway, 13–15 June 2017; Axel, M., Nanna, R.-S., Eds.; Abstracts and Proceedings of the Geological Society of Norway. Norsk Geologisk Forening: Trondheim, Norway, 2017; Volume 2, pp. 97–99.
39. Pieczka, A.; Włodek, A.; Gołębiowska, B.; Szełęg, E.; Szuszkiewicz, A.; Ilnicki, S.; Nejbert, K.; Turniak, K. Phosphate-bearing pegmatites in the Góry Sowie Block and adjacent areas, Sudetes, SW Poland. In Proceedings of the 7th International Symposium on Granitic Pegmatites PEG 2015, Książ, Poland, 17–19 June 2015; Book of Abstracts. Adam, S., Jan, C., Eds.; Tigris: Zlín, Czech Republic, 2015; pp. 77–78.
40. Stormer, J.C.; Pierson, M.L.; Tacker, R.C. Variation of F and Cl X-ray Intensity Due to Anisotropic Diffusion in Apatite during Electron Microprobe Analysis. *Am. Mineral.* **1993**, *78*, 641–648. Available online: http://www.minsocam.org/ammin/AM78/AM78_641.pdf (accessed on 14 April 2018).
41. Goldoff, B.; Webster, J.D.; Harlov, D.E. Characterization of fluor-chlorapatites by electron probe microanalysis with a focus on time-dependent intensity variation of halogens. *Am. Mineral.* **2012**, *97*, 1103–1115. [CrossRef]
42. Suitch, P.R.; Lacout, J.L.; Hewat, A.W.; Young, R.A. The structural location and role of Mn^{2+} partially substituted for Ca^{2+} in fluorapatite. *Acta Crystallogr.* **1985**, *41*, 173–179. [CrossRef]
43. Ercit, T.S.; Tait, K.T.; Cooper, M.A.; Abdu, Y.; Ball, N.A.; Anderson, A.J.; Černý, P.; Hawthorne, F.C.; Galliski, M. Manitobaite, Na16 Mn^{2+}25Al8(PO4)30, a new phosphate mineral species from Cross Lake, Manitoba, Canada. *Can. Mineral.* **2010**, *48*, 1455–1463. [CrossRef]
44. Tait, K.T.; Hawthorne, F.C.; Černý, P.; Galliski, M.A. Bobfergusonite from the Nancy pegmatite, San Luis Range, Argentina: Crystal-structure refinement and chemical composition. *Can. Mineral.* **2004**, *42*, 705–716. [CrossRef]
45. Papike, J.J.; Jensen, M.; Laul, J.C.; Shearer, C.K.; Simon, S.B.; Walker, R.J. Apatite as a recorder of pegmatite petrogenesis. *Geol. Soc. Am. Abstr. Programs* **1984**, *16*, 617.
46. Černý, P.; Fryer, B.J.; Chapman, R. Apatite from Granitic Pegmatite Exocontact in Moldanubian Serpentinites. *J. Czech Geol. Soc.* **2001**, *46*, 15–20. Available online: http://www.jgeosci.org/detail/JCGS.814 (accessed on 17 January 2018).
47. Włodek, A.; Grochowina, A.; Gołębiowska, B.; Pieczka, A. A phosphate-bearing pegmatite from Lutomia and its relationship to other pegmatites of the Góry Sowie Block, southwestern Poland. *J. Geosci.* **2015**, *60*, 45–72. [CrossRef]
48. Grochowina, A. Mineralogical Study of Phosphate-Bearing Pegmatites from Michałkowa in the Sowie Mts. Ph.D. Thesis, AGH University of Science and Technology, Kraków, Poland, 2016. (In Polish with Abstract in English).
49. Thomas, R.; Webster, J.D.; Heinrich, W. Melt inclusions in pegmatite quartz: Complete miscibility between silicate melts and hydrous fluids at low pressure. *Contrib. Mineral. Petrol.* **2000**, *139*, 394–401. [CrossRef]
50. Veksler, I.V.; Thomas, R. An experimental study of B-, P- and F-rich synthetic granite pegmatite at 0.1 and 0.2 GPa. *Contrib. Mineral. Petrol.* **2002**, *143*, 673–683. [CrossRef]
51. Simmons, W.B.; Webber, K.L. Pegmatite genesis: State of the art. *Eur. J. Mineral.* **2008**, *20*, 421–438. [CrossRef]
52. Thomas, R.; Davidson, P.; Beurlen, H. The competing models for the origin and internal evolution of granitic pegmatites in the light of melt and fluid research. *Mineral. Petrol.* **2012**, *106*, 55–73. [CrossRef]
53. Novák, M.; Gadas, P.; Kocáb, J. Secondary beryl in cordierite/sekaninaite pseudomorphs—An indicator of elevated content of beryllium in the precursor. In Proceedings of the 8th International Symposium on Granitic Pegmatites PEG 2017, Kristiansand, Norway, 13–15 June 2017; Axel, M., Nanna, R.-S., Eds.; Abstracts and Proceedings of the Geological Society of Norway. Norsk Geologisk Forening: Trondheim, Norway, 2017; Volume 2, pp. 97–99.
54. Wojtulek, P.M. The Non-Serpentine Phases as the Indicators of Evolution of Serpentinite Members of the Lower Silesia Ophiolites. Ph.D. Thesis, University of Wroclaw, Wroclaw, Poland, 2016. (In Polish with Abstract in English).
55. Sharp, Z.D.; Barnes, J.D. Water-soluble chlorides in massive seafloor serpentinites: A source of chloride in subduction zones. *Earth Planet. Sci. Lett.* **2004**, *226*, 243–254. [CrossRef]
56. Bonifacie, M.; Busigny, V.; Mével, C.; Philippot, P.; Agrinier, P.; Jendrzejewski, N.; Scambelluri, M.; Javoy, M. Chlorine isotopic composition in seafloor serpentinites and high-pressure metaperidotites. Insights into oceanic serpentinization and subduction processes. *Geochim. Cosmochim. Acta* **2008**, *72*, 126–139. [CrossRef]

57. John, T.; Scambelluri, M.; Frische, M.; Barnes, J.D.; Bach, W. Dehydration of subducting serpentinite: Implications for halogen mobility in subduction zones and the deep halogen cycle. *Earth Planet. Sci. Lett.* **2011**, *308*, 65–76. [CrossRef]
58. Kendrick, M.A.; Honda, M.; Pettke, T.; Scambelluri, M.; Phillips, D.; Giuliani, A. Subduction zone fluxes of halogens and noble gases in seafloor and forearc serpentinites. *Earth Planet. Sci. Lett.* **2013**, *365*, 86–96. [CrossRef]